ACS Catalysis

Research Article

pubs.acs.org/acscatalysis

Topotactic Transformation of Zeolite Supported Cobalt(II) Hydroxide to Oxide and Comparison of Photocatalytic Oxygen Evolution

Joselyn Del Pilar-Albaladejo and Prabir K. Dutta*

Department of Chemistry and Biochemistry, The Ohio State University, 120 W. 18th Avenue, Columbus, Ohio 43210, United States

Supporting Information

ABSTRACT: A synthesis method that results in ~180 nm plate-like crystallites of β-$(Co(OH)_2$ anchored on the surface of zeolite Y particles is reported. These crystals of β-$Co(OH)_2$ are transformed to Co_3O_4 by thermal treatment without a change in morphology. Characterization of the cobalt phases and the transformation was carried out by powder X-ray diffraction, X-ray photoelectron spectroscopy, Raman spectroscopy, and electron microscopy. These cobalt-based materials provide an opportunity to contrast their photocatalytic activity. Using the $Ru(bpy)_3^{2+}$–persulfate system, the oxidation of water to oxygen was measured. The most active catalyst was β-$(Co(OH)_2$, and with transformation to Co_3O_4, the catalytic activity declined, suggesting that β-$Co(OH)_2$ is a better photocatalyst than Co_3O_4. The photocatalytic activity of the β-$(Co(OH)_2$/zeolite decreased during a second photocatalytic cycle, due to surface transformation to Co_3O_4, though the bulk of the catalyst still maintains the brucite-like β-$Co(OH)_2$ structure. This is the first report on how catalytic activity is altered in the cobalt oxide system by phase transformation, keeping morphological features unchanged.

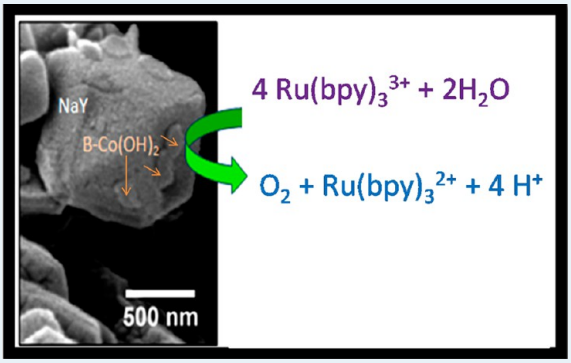

KEYWORDS: *water oxidation, zeolite Y, transition metal photocatalysis, metal hydroxides, cobalt clusters*

INTRODUCTION

Photolytic oxidation of water to oxygen, especially in the context of artificial photosynthetic systems, is an active area of research. Since water oxidation is a multiple electron process, catalysts are essential. Development of heterogeneous catalysts, especially the oxides of Ir, Ru, Co, and Mn, has a long history.[1−6] Cobalt hydroxides and oxides on nanosilica,[5] mesoporous silica,[7−9] alumina, aluminosilicates, and titania[10] have been reported. Colloidal hydroxides are typically unstable in a buffer but can be stabilized if fixed on supports.[10] The use of supports also minimizes catalyst aggregation and can modify the acidic properties of the catalyst including assisting deprotonation of the hydroxyl groups on the cobalt oxide surface.[7,10]

We report here the synthesis of β-cobalt(II) hydroxides on the surface of zeolite particles (as compared to the zeolite interior) and thermal treatment to the stable spinel Co_3O_4 and their catalytic activity toward water oxidation. The motivation for this work is two-fold. First, zeolite Y, because of its ion-exchanging properties, provides a novel nonimpregnation route for the synthesis of cobalt hydroxide on its surface. Second, catalysts formed on the zeolite surface can be exploited for artificial photosynthetic systems using zeolite membranes. In this architecture, photoactive species incorporated within the zeolite membrane lead to charge separated species upon illumination that migrate to the opposite surfaces of the membrane. Catalysts on the two opposite surfaces of the zeolite membrane can regenerate the photoactive species with the formation of relevant photoproducts. We have reported on such a system that incorporated nanotubular RuO_2 on a zeolite membrane surface which was a catalyst for water to hydrogen production using sacrificial agents.[11] The motivation of the present research is to develop water oxidation catalysts on zeolite particle surfaces, which after optimization can be made on zeolite membrane surfaces. We report in this paper detailed characterization of the cobalt species formed on the zeolite surface using spectroscopy and electron microscopy. The activity toward oxygen evolution was measured using photolytically generated $Ru(bpy)_3^{3+}$ using persulfate as the sacrificial electron acceptor.

EXPERIMENTAL SECTION

Synthesis of Zeolite-Supported Cobalt Catalyst. Commercial zeolite Y was purchased from Zeolyst International Si/Al = 2.5. A total of 500 mg of zeolite Y was ion-exchanged for 2 h at 25 °C under constant stirring with 50 mL of 0.01 M $CoCl_2$. The pink solid was then filtered and washed with deionized (DI) water. The Co-exchanged sample was treated with 50 mL of 0.1 M NaOH. A blue color was initially observed; after 2 h in an oil bath at 90 °C, the solid changed color to a light brown. The recovered solid was then filtered, washed, and dispersed in 50 mL of deionized water and stirred at 90 °C for 24 h. This material is identified as Co/Y-25.

Received: June 19, 2013
Published: November 22, 2013

Catalysts identified by Co/Y-125 and Co/Y-400 were made by thermal annealing of Co/Y-25 for 24 h at 125 and 400 °C, respectively. All samples were stored ~0 °C, as a precaution to avoid any slow oxidation processes.

Characterization. Catalysts were characterized by powder X-ray diffraction (XRD), Raman spectroscopy, X-ray photoelectron spectroscopy (XPS), and electron microscopy. XRD was studied using a Rigaku X-ray Diffractometer with Cu Kα radiation. Data were collected using a 0.50 divergence and scatter slits 10 receiving slit. The scan mode was used with a 0.014 step size and 0.5 s dwell time. Raman spectra were acquired using a 785 nm laser line at 0.5% power, using a Renishaw Raman microprobe. The use of a spinning cell was necessary to preserve sample integrity. XPS spectra were acquired utilizing the Axis Kratos X-ray Photoelectron Spectrometer. The X-ray source selected was a monochromatized Al K_α source (12 kV, 10 mA). Region scans were collected using a 20 eV pass energy. Peak positions were calibrated relative to C 1s peak position at 285.0 eV. Scanning electron micrographs were obtained using XL-30 ESEM FEG (Environmental SEM) (Field Emission Gun). Cobalt samples were coated with a thin layer of evaporated gold for 60 s, and secondary electron microscopy images were obtained. Transmission micrographs were acquired using Titan3 80−300 Probe-Corrected Monochromated (S) at low voltages (~140 kV).

Elemental Analysis. Digestion of zeolite-supported catalysts was based on a previous cold digestion method.[12] Briefly, 10 mL of an equal parts solution containing HNO_3, HCl, and HF was added to a preweighed Teflon bottle containing 50 mg of catalyst. After dissolution, 75 mL of ~0.86 M boric acid was added to the clear solution to neutralize HF. Deionized water was then added until the weight was 100 g. Cobalt loading was then determined by atomic absorption spectroscopy (AAS).

Photocatalytic Water Oxidation. The dissolved oxygen measurements were recorded using a YSI Instruments Clark Oxygen electrode which was calibrated using 100% air saturated DI water at 25 °C (8.26 ppm) before each catalysis. A Pyrex photolysis reactor containing 0.333 mg of sodium persulfate (0.02 M, 70 mL), 0.994 g of sodium sulfate (0.1 M, 70 mL), 0.0059 mg of tris(2,2′-bipyridyl) ruthenium chloride, 0.050 g of catalyst in a Na_2HPO_4−$NaHCO_3$ (pH 5.7−6.0) buffer was purged with nitrogen gas for 15 min while stirring or until baseline reading was 0.0−0.10 ppm. The reactor was illuminated with visible light using a Hg lamp equipped with a 420 nm cutoff filter and with a power of 360 mW/cm^2 incident on the photocatalytic system described above.

RESULTS AND DISCUSSION

Generation of Photocatalysts. Zeolite Y as a support provides a novel route for synthesis of the cobalt hydroxide. The synthesis method involved treating Co^{2+} ion-exchanged zeolite Y with 0.1 M NaOH. The strategy was that as Co^{2+} ions are exchanged out of the zeolite by Na^+, they would precipitate on the zeolite surface because of the [OH^-] in solution. Further hydrothermal treatment was done to ensure anchoring the material on the zeolite surface. Thermal annealing in the air for 24 h was done at various temperatures; the reported data primarily focus on Co/Y-25 (as prepared) and Co/Y-125, Co/Y-400 annealed at 125 and 400 °C, respectively.

Characterization of Photocatalysts. The Co content of all samples was determined by atomic absorption spectroscopy. A low temperature digestion method was used to dissolve the zeolite. The elemental analysis is shown in Table 1, and Co/Y-25, Co/Y-125, Co/Y-400 contain 2.9, 2.6, and 2.9 wt % of cobalt and, as expected, is similar for all the samples. Raman spectra shown in Figure 1 indicate a marked difference between Co/Y-25 and Co/Y-125 and Co/Y-400 samples. In the Co/Y-25 sample (Figure 1a), the peaks are primarily those of zeolite Y (300, 360, and 503 cm^{-1}).[13] For Co/Y-125 and Co/Y-400, the spectra are dominated by characteristic bands of Co_3O_4 at 194 (F_{2g}), 485 (E_g), 624 (F_{2g}), and 694 (A_{1g}) cm^{-1}.[14] The zeolite framework band at 503 cm^{-1} is dwarfed by the bands of Co_3O_4. Powder X-ray diffraction (XRD) patterns shown in Figure 2 indicate diffraction peaks corresponding to zeolite Y in all Co/Y samples (Figure 2a−c). In the Co/Y-25 (Figure 2a), peaks at 19°(002) arise from β-$Co(OH)_2$ (JCPDS File Card No. 30-0443, also matches a pure sample of β-$Co(OH)_2$ shown in Figure 2e). In the case of Co/Y-125 and Co/Y-400, this peak

Table 1. Cobalt Loadings Obtained by AAS

catalyst	%w/w
25	2.9
recovered	2.7
125	2.6
400	2.9

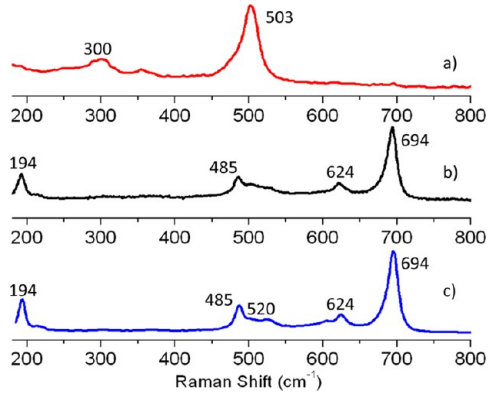

Figure 1. Raman spectra for (a) Co/Y-25 (as prepared), (b) Co/Y-125, and (c) Co/Y-400.

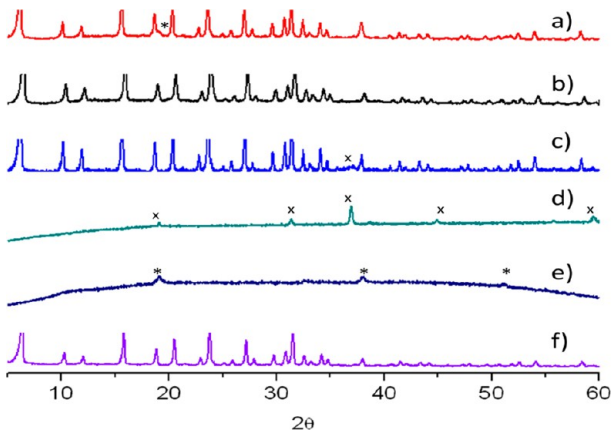

Figure 2. Powder X-ray diffraction (XRD) patterns of (a) Co/Y-25 (∗ indicates a peak at 19°), (b) Co/Y-125, (c) Co/Y-400 (x indicates peak at 37°), (d) Co_3O_4 e) β-$Co(OH)_2$, and (f) zeolite Y.

dx.doi.org/10.1021/cs400991v | ACS Catal. 2014, 4, 9−15

disappears, but no new peaks are apparent (a weak peak at 37° in Figure 1c).

Since the XRD of Co/Y-125 did not exhibit the Co_3O_4 peak (37° 2θ), yet the Raman signal was strong, indicating Co_3O_4, we carried out an analysis that compared the sensitivity of the two techniques. Figure 3 compares the XRD and Raman spectra of physical mixtures of Co_3O_4 and zeolite Y. It is clear that with the 1 wt % of Co_3O_4, the XRD peak of Co_3O_4 is very weak (marked in Figure 3c), and this peak is not observable at concentrations below 0.5 wt % Co_3O_4 (Figure 3d is the XRD of 0.01 wt %), whereas Raman spectroscopy of 0.1 wt % (Figure 3a) as well as that of 0.01 wt % Co_3O_4 (Figure 3b) clearly exhibits the bands at 194, 485, 624, and 694 cm^{-1}, indicating that the strong Raman cross-section of Co_3O_4 can be useful for analysis of low levels of Co_3O_4. A previous study of Co_3O_4 on mesoporous silica also noted that the XRD pattern was not observed, whereas the Raman exhibited the characteristic Co_3O_4 peaks.[9]

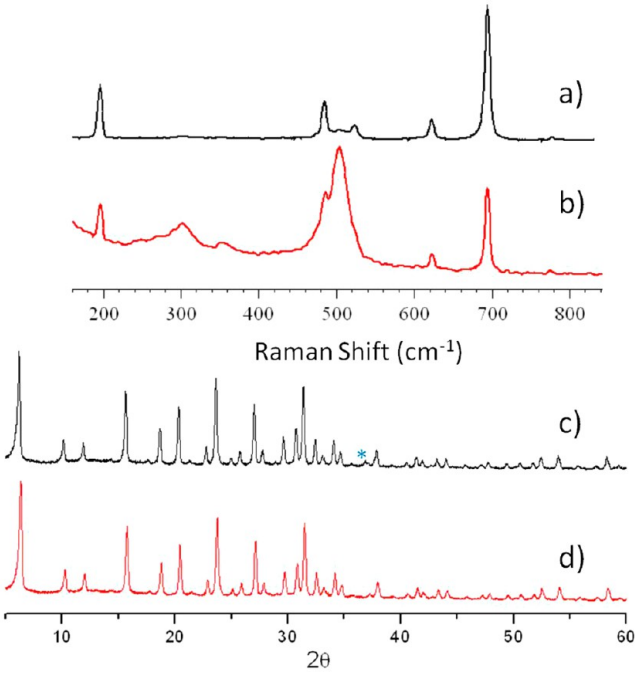

Figure 3. Raman spectra of mixtures Co_3O_4 and zeolite Y (a) 1% w/w of Co_3O_4, (b) 0.01% w/w Co_3O_4. XRD pattern of mixtures Co_3O_4 and zeolite Y, (c) 1% w/w of Co_3O_4 (peak at 37° is marked), (d) 0.01% w/w Co_3O_4.

The broad multielectron excitation satellite shake up peaks in the Co 2p region of the X-ray photoelectron spectra (XPS) are used to distinguish between Co(II) and Co(III) compounds.[15] Figure 4 is the XPS of the three samples in the Co $2p_{1/2}$ (>792 eV) and the Co $2p_{3/2}$ (775−790 eV) regions. The presence of a satellite line at 785.1 eV is indicative of the Co(II).[16] For both Co/Y-125 and Co/Y-400 (Figure 4b,c), the satellite peaks are weaker (a decrease of 30% relative to Co $2p_{3/2}$ peak), and there is broadening of the XPS peaks, indicative of the formation of Co(III).

Figure 5 shows the SEM of the as-prepared sample and upon subsequent thermal treatment. For all of the samples, well dispersed plate-like clusters (marked by arrows) are observed on the zeolite surface with comparable size and morphology between samples. The size of these deposited particles was measured (~ 100 particles), and from the histogram (Figure S1 in Supporting Information), an average size for the particles was calculated. For samples Co/Y-25 and Co/Y-125, the size peaked at ~180 nm, and for Co/Y-400, it peaked at 100 nm.

Figure 6 shows the HRTEM of these samples, with particular focus on the deposited particles on the zeolite surface (we have also included the Co/Y-100 sample). Figure 6a,c,e,g show the

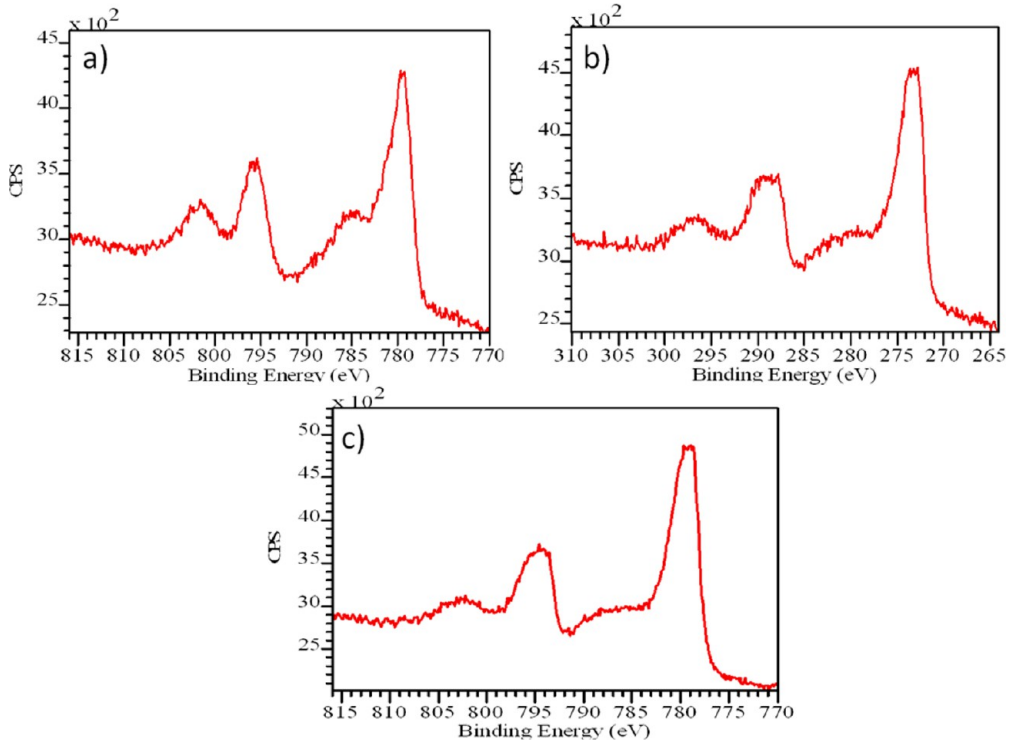

Figure 4. X-ray photoelectron spectroscopy of (a) Co/Y-25 (as prepared), (b) Co/Y-125, and (c) Co/Y-400.

dx.doi.org/10.1021/cs400991v | ACS Catal. 2014, 4, 9−15

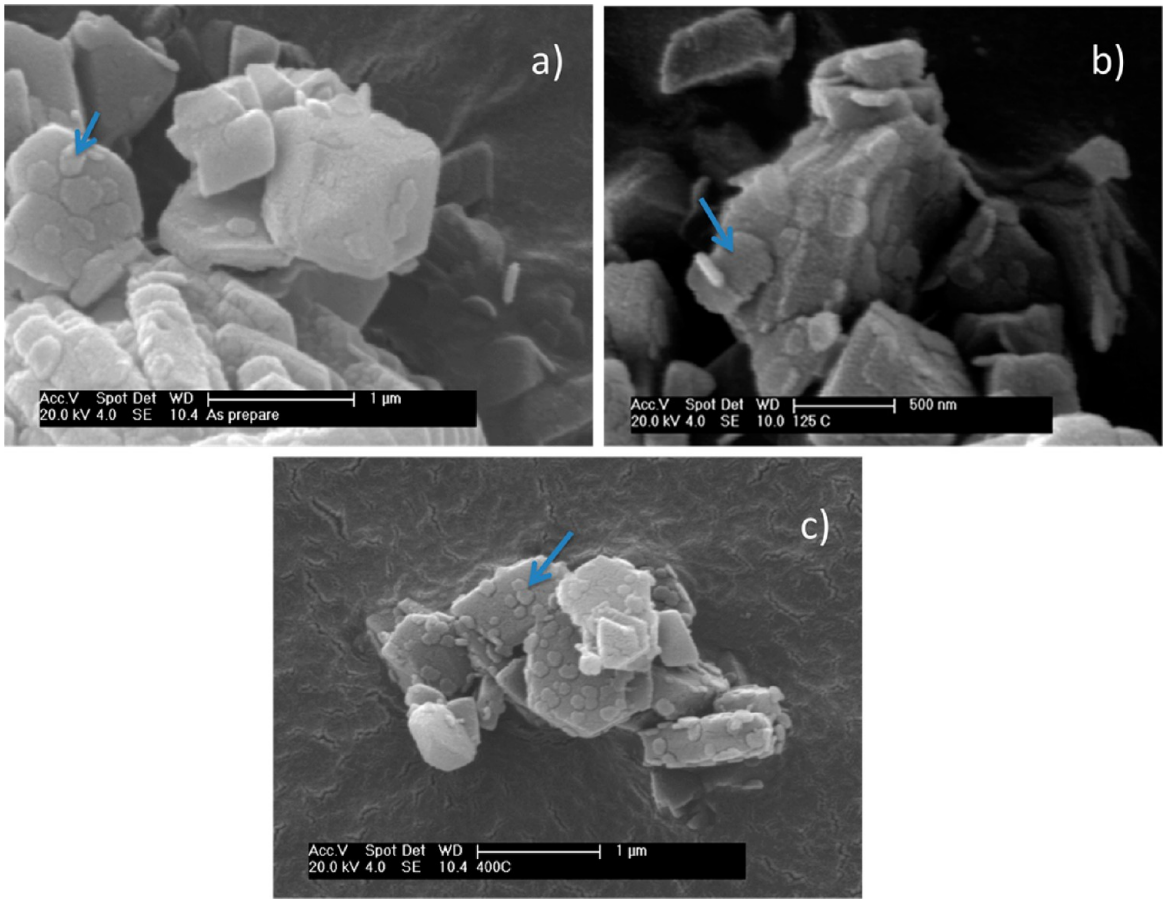

Figure 5. Representative SEM micrographs of (a) Co/Y-25 (as prepared), (b) Co/Y-125, and (c) Co/Y-400 (arrows point to the platelet-like structures deposited on the zeolite crystals).

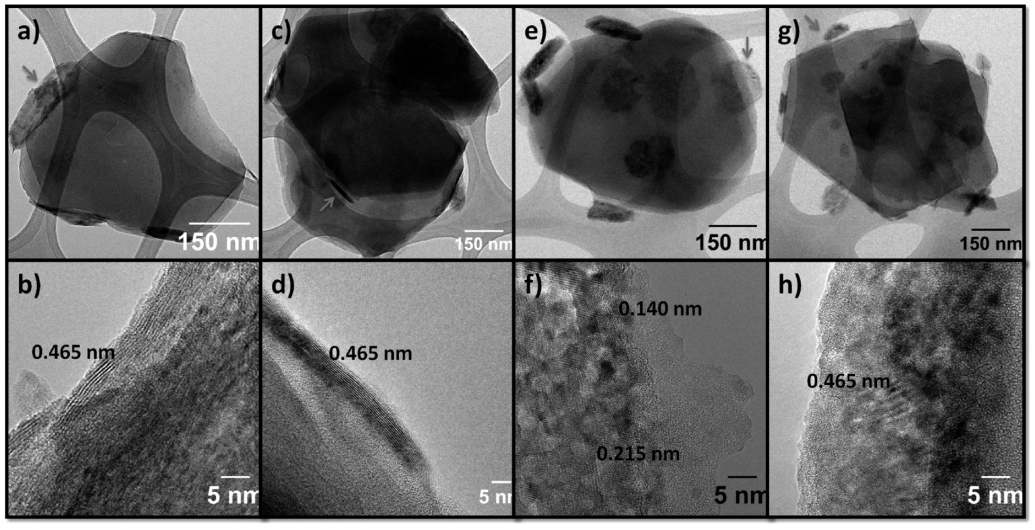

Figure 6. TEM micrographs (a,b) Co/Y-25 (as prepared), (c,d) Co/Y-100, (e,f) Co/Y-125, and (g,h) Co/Y-400 (arrows show the deposits on the surface of the zeolite Y particle). HRTEM images in b, d, f, and h indicate the fringes spacing for each cluster.

entire zeolite particle with deposits on the surface of the zeolite, and Figure 6b,d,f,h are higher resolution micrographs focused on the deposited particle. From Figure 6b for Co/Y-25, the electron micrograph indicates that the material deposited on the zeolite surface is layer-like and crystalline, as evident from the lattice fringes, and resembles a previous HRTEM of β-$Co(OH)_2$.[17] The *d*-spacings calculated for Co/Y-25 were found to be 0.46 nm, assigned to the (001) plane of β-$Co(OH)_2$.[18] The *d*-spacing of the layered like deposit with a spacing of 0.46 nm was also found in Co/Y-100 (Figure 6d). The Co/Y-125 sample (Figure 6f) showed diffraction fringes with multiple spacings; it was no longer layer-like; the *d*-spacings of 0.22 and 0.14 nm are in agreement with the *d*-spacings reported for the (220) and (511) crystal planes in spinel Co_3O_4.[15] For Co/Y-

dx.doi.org/10.1021/cs400991v | *ACS Catal.* 2014, 4, 9−15

400, we observed spacings of 0.46 nm due to the (111) crystal plane of Co_3O_4. All of the deposits had cobalt in them, based on energy dispersive elemental analysis.

On the basis of these the characterization data, we conclude that cobalt in samples Co/Y-25 is primarily crystalline β-$Co(OH)_2$; for Co/Y-125 and Co-Y/400, the material is Co_3O_4. Previous thermal analysis studies have shown that β-$Co(OH)_2$ transforms to Co_3O_4 at 130 °C via dehydroxylation.[19] The topotactic transformation of β-$Co(OH)_2$ into Co_3O_4 upon thermal treatment with preservation of the plate-like morphology has also been reported with free nanoparticles of these materials.[15]

Photocatalytic Performance. *Fresh Catalysts.* Photocatalytic performance toward water oxidation for all three materials was examined using tris(2,2′-bipyridine)ruthenium(II), $Ru(bpy)_3^{2+}$, as a photosensitizer and persulfate as the sacrificial electron acceptor in a NaH_2PO_4–$NaHCO_3$ (pH 6) buffered system. The formation of dissolved oxygen was measured using a Clark oxygen electrode. Our focus on this study was to evaluate how the catalytic activity changes between the samples, keeping all experimental conditions the same. Figure 7 contrasts the oxygen evolution data. The initial

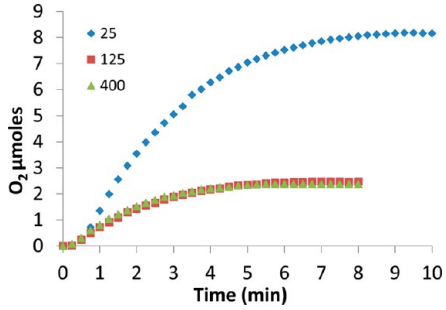

Figure 7. Visible light-induced oxygen evolution for Co/Y-25 (as prepared), Co/Y-125, and Co/Y-400, all three catalysts over time (dissolved oxygen measured with a Clark electrode).

oxygen evolution rates (OER; first 4 min) are 1.92 ± 0.3, 0.43 ± 0.2, and 0.56 ± 0.02 μmol/min, with the photocatalytic activity following the trend Co/Y-25 > Co/Y-125 ~ Co/Y-400. The oxygen evolution for the Co/Y-25 sample was also examined at pH 7 and 8, and these data are shown in Figure S2. The optimum pH was at 7, with an initial rate of 2.80 μmol/min and dropped to 0.78 μmol/min at pH 8. Water oxidation is thermodynamically favored at higher pH. However the photodecomposition of $Ru(bpy)_3^{3+}$ is also promoted at higher pH and explains the observation that the optimum pH for O_2 evolution is observed around pH 7.

Focusing on the Co/Y-25 sample, which gave the best results, we address several issues. First, the amount of oxygen evolved at a steady state is ~8 μmol, which is significantly less than the maximum amount of oxygen that can be generated based on the amount of $S_2O_8^{2-}$ that is used (total possible oxygen ≈ 700 μmol, dissolved oxygen at saturation ≈ 88 μmol). Most previous studies with the cobalt-based photocatalysts have noted that the amount of O_2 evolved at a steady state is less than the theoretical amount, the divergence depending on several factors, including the amount of catalyst used. For example, with $LaCoO_3$, the amount of O_2 evolved varied from 74% (Co-0.12 mg/mL) to 14% (Co-0.006 mg/mL).[20] With Co-aluminophosphates, also a microporous material like zeolite, the amount of oxygen evolved is 11.5% (Co-0.2 mg/mL).[8] Our experiments are done with low levels of active catalytic material (Co, 0.014 mg/mL), and thus, expectedly, the steady-state O_2 yields are low. Second, the catalyst ceases functioning after 5–6 min; such observations are also very common in the literature, for water photooxidation of $Ru(pby)_3^{2+}$ using sacrificial $S_2O_8^{2-}$ ions. Solution-phase measurements show saturation within minutes, whereas gas-phase measurements of O_2 usually show saturation within 10–20 min, well before the stoichiometric amounts of O_2 are evolved. There are several reasons for these observations. First, the concentration of $Ru(bpy)_3^{2+}$ in the solution decreases due to photodecomposition. We note with Co/Y-25 that after 10 min photolysis, about 19% of the $Ru(bpy)_3^{2+}$ is decomposed (Figure S3). A second possibility is that the catalyst surface is getting contaminated, dissolving or transforming to something else. To examine this further, the recovered catalyst was washed well and characterized by several techniques and then re-examined for its photocatalytic ability.

Recovered Catalysts. Figure 8 shows that the photocatalytic performance of Co/Y-25, when used in a second photolytic

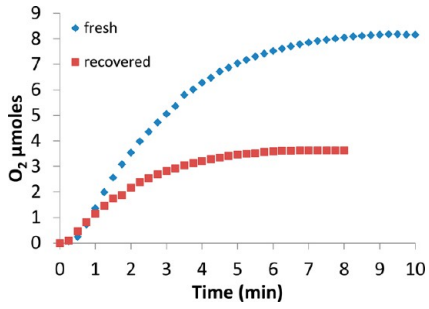

Figure 8. Comparison of the oxygen evolution ability of Co/Y-25 (as prepared) and after going through a photocatalytic cycle.

cycle, clearly shows that the catalyst performance is degraded. Elemental analysis (Table 1) shows that the Co content of the recovered catalysts is 2.7 wt %, a slight decrease, and cannot account for the decreased catalytic activity. Figure 9 shows the electron micrographs of the recovered catalyst. The STEM image in Figure 9c shows the presence of platelets on the zeolite surface, similar to what was observed in the parent Co/Y-25. Figure 9d shows the cobalt distribution on the zeolite surface, and indicates that the surface deposits are cobalt-containing compounds, the same pattern for the as-synthesized Co/Y-25. The high-resolution TEM images in Figure 9a,b indicate that the platelets still maintain the layered structure of β-$Co(OH)_2$, also present in the starting sample (Figure 6b). Thus, from an elemental and morphological perspective, there do not appear to be significant differences between the parent and recovered catalysts.

Figure 10a,b show the Raman and XPS of the recovered catalyst, respectively. The Raman spectrum shows the presence of Co_3O_4, as evidenced by the bands at 194 and 694 cm^{-1}, which were not present on the original Co/Y-25 sample (Figure 1a). Using the relative ratios of the zeolite band (503 cm^{-1}) and the 692 cm^{-1} band, and the intensities of the mixtures of Co_3O_4 and zeolite Y shown in Figure 3a,b, we estimate a loading of <0.01 wt % of Co_3O_4, which translates to the fraction of the cobalt present as Co_3O_4 as <0.4% of the entire cobalt sample. The XPS data in Figure 10a also suggest the formation of Co(III), because of the decrease of the intensity of the satellite peak (compare to Figure 4a). Thus, the

dx.doi.org/10.1021/cs400991v | ACS Catal. 2014, 4, 9–15

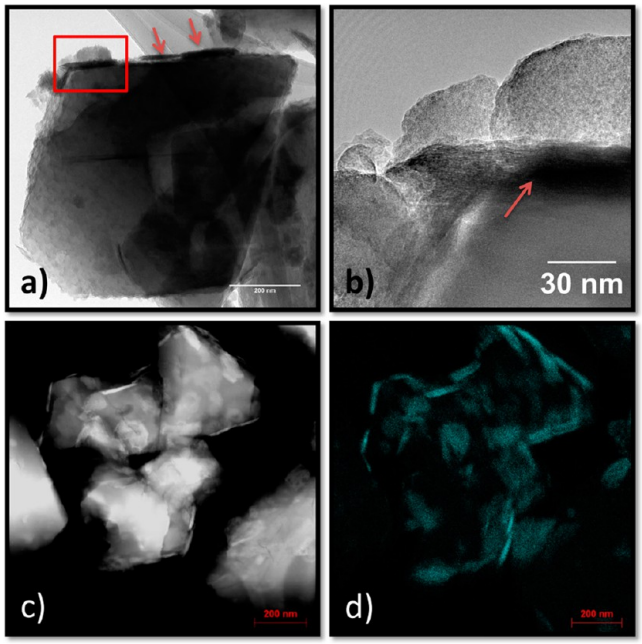

Figure 9. TEM micrographs for the Co/Y-25 recovered after a photolytic cycle. (a,b) Arrows indicate the layered cobalt hydroxide structure anchored onto the zeolite surface. Micrograph (b) shows the HRTEM of the area within the square in image (a). STEM images of the (c) recovered Co/Y-25 sample and (d) a cobalt elemental analysis map, indicating that the layered structures are cobalt containing clusters on the zeolite surface.

spectroscopic analysis suggests that the surface of the β-$Co(OH)_2$ is being converted to Co_3O_4 during the photolysis reaction, though the bulk retains the β-$Co(OH)_2$ structure. The conversion of the surface of CoO to an epitaxial layer of Co_3O_4 under oxidizing conditions has been reported.[21] The loss in catalytic activity of the recovered Co/Y-25 is explained by its surface conversion to Co_3O_4, since as the data in Figure 7 suggest, thermal annealing to the Co_3O_4 in Co/Y-125 and Co/Y-400 leads to lower oxygen evolution. Oxidation of the active metal site (Fe^{2+}) with a loss of catalytic performance has been noted for Fe_3O_4.[22]

Comparison of the present zeolite-based catalyst with other studies, especially using TOF calculations, is fraught with difficulties, more so when comparing lamp and laser-based photolysis experiments.[23] To get some idea of the efficacy of the present catalysts, we compared the initial rates reported in the literature per unit weight of cobalt used. For the Co/Y-25, Co/Y-125, and Co/Y-400, these numbers are 19.8, 7.4, and 6.4 μmol O_2/s g Co. An example of a recent Co_3O_4-based catalyst found 13.9 μmol O_2/s g Co.[20] Other reported studies with Co_3O_4 also lead to comparable numbers.[3,22,24] Thus, our overall catalytic performance is comparable to other cobalt-based systems.

Mechanistic Aspects. The β-$Co(OH)_2$ plates formed on the zeolite surface in Co/Y-25 undergo a topotactic phase transformation to spinel Co_3O_4 in samples Co/Y-125 and Co/Y-400, and the catalytic activity decreases. Early work focused on $Co^{III}(OH)_3$ indicated that catalytic activity decreased as the hydroxide was converted to oxide, though morphological studies were not reported.[10] More recently, 1−2 nm $Co^{II}(OH)_2$ supported on SiO_2 nanoparticles exhibited a remarkably high catalytic activity for oxygen using the oxidant $Ru(bpy)_3^{3+}$.[5]

The mechanism of water oxidation to oxygen on heterogeneous cobalt-based catalysts is being debated, and why the hydroxide is a better catalyst than the oxide, even though both particles are of similar morphologies, is at present unclear. The relevant structural differences between the hydroxide and the oxide are the spacing of Co atoms in framework and the acidic hydroxyl groups in the hydroxide. Stopped-flow kinetic data for starch-stabilized colloidal cobalt-(III) hydroxides as water oxidation catalysts and electrokinetic studies suggest that the O−O formation happens between two adjacent cobalt active centers.[25,26] In the brucite-like structure of β-$Co(OH)_2$, the hydroxyl ions are packed in a hexagonal geometry with cobalt atoms present in alternate rows of octahedral sites. The Co−Co interatomic distance in $Co(OH)_2$ supported on kaolinite has been reported to be 3.173 Å.[27] For the spinel Co_3O_4, the structure consists of cubic close-packed O^{2-} ions with Co(II) and Co(III) in tetrahedral and Co(III) octahedral sites, respectively; the distance between two cobalt atoms in the spinel is between 3.07 and 3.21 Å.[28] Besides the Co−Co distances, the other aspect that is important is the active crystal phase involved in the photocatalytic reaction. For example, it has been shown that certain faces of Co_3O_4 are most active in CO oxidation, with the (110) being more active than the (001) and (111) planes, primarily because there are more exposed Co(III) atoms in the (110) site.[29] Thus, both structural aspects as well as the crystal morphology could be playing a role in the different photocatalytic activity between the Co/Y-25 and the Co/Y-125 and Co/Y-400 samples.

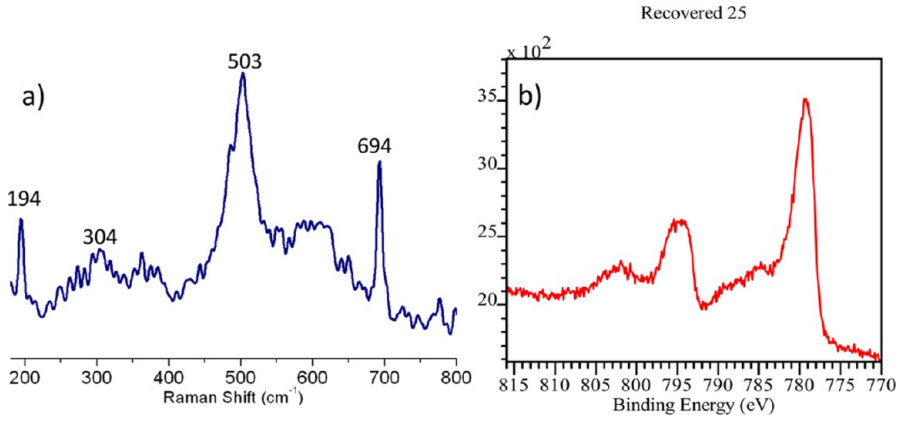

Figure 10. (a) Raman spectrum and (b) XPS of catalyst recovered after photolysis.

dx.doi.org/10.1021/cs400991v | ACS Catal. 2014, 4, 9−15

In summary, we have successfully synthesized ∼180 nm crystalline brucite-like cobalt hydroxides anchored on zeolite, which undergo a phase transition to spinel Co_3O_4 at temperatures of 125 °C, retaining the overall shape and morphology. The strategy for synthesis which exploits the ion-exchanging properties of the zeolite, followed by precipitation and hydrothermal treatment, leads to $Co(OH)_2$ that is secured on the zeolite surface and should minimize detachment of the catalyst particles, a problem that has been noted with previous supports.[25] An advantage of the surface deposition on the zeolite support is that the oxidant has ready access to the catalyst, and issues of migration through a porous network are absent and can be adapted to zeolite membranes. An advantage of the negative charge of the zeolite surface is that $Ru(bpy)_3^{2+}$ is attracted to the zeolite scaffold. The photocatalytic activity is more pronounced for the β-$Co(OH)_2$ sample, as compared to Co_3O_4, with both samples of similar particle morphology and size. The β-$Co(OH)_2$ catalyst decreases in activity after the first photocatalytic cycle, and electron microscopy and spectroscopic studies indicate that there is a surface modification upon going through the photocatalytic cycle to form Co_3O_4. Efforts are underway to examine the catalytic activity as the size of the deposited particles is gradually decreased.

■ ASSOCIATED CONTENT

Supporting Information

The size histograms based on the SEM micrographs, pH-dependence oxygen evolution, and the UV−vis decomposition spectra for the Co/Y-25 photocatalytic experiment. This information is available free of charge via the Internet at http://pubs.acs.org/.

■ AUTHOR INFORMATION

Corresponding Author

*E-mail: dutta.1@osu.edu.

Notes

The authors declare no competing financial interest.

■ REFERENCES

(1) Hara, M.; Mallouk, T. E. *Chem. Commun.* **2000**, 1903−1904.
(2) Das, S. K.; Dutta, P. K. *Microporous Mesoporous Mater.* **1998**, *22*, 475−483.
(3) Jiao, F.; Frei, H. *Angew. Chem., Int. Ed.* **2009**, *48*, 1841−1844.
(4) Iyer, A.; Del-Pilar, J.; King'ondu, C. K.; Kissel, E.; Garces, H. F.; Huang, H.; El Sawy, A. M.; Dutta, P. K.; Suib, S. L. *J. Phys. Chem. C* **2012**, *116*, 6474−6483.
(5) Zidki, T.; Zhang, L.; Shafirovich, V.; Lymar, S. V. *J. Am. Chem. Soc.* **2012**, *134*, 14275−14278.
(6) Jiao, F.; Frei, H. *Energy Environ. Sci.* **2010**, *3*, 1018−1027.
(7) Yusuf, S.; Jiao, F. *ACS Catal.* **2012**, *22*, 2753−2760.
(8) Armandi, M.; Hernandez, S.; Vankova, S.; Zaranilli, S.; Boneli, B.; Garrone, E. *ACS Catal.* **2013**, *3*, 1272−1278.
(9) Hyun, S. A.; Yano, J.; Tilley, T. D. *Energy Environ. Sci.* **2013**, *6*, 3080−3087.
(10) Elizarova, G. L.; Zhidomirov, G. M.; Parmon, V. *Catal. Today* **2000**, *58*, 71−88.
(11) Kim, Y.; Dutta, P. K. *J. Phys. Chem. C* **2007**, *111*, 10575−10581.
(12) Peru, D. A.; Collins, R. J. *Fresenius' J. Anal. Chem.* **1993**, *346*, 909−913.
(13) Twu, J.; Dutta, P. K.; Kresge, C. T. *Zeolites* **1991**, *11*, 672−679.
(14) Hadjiev, V. G.; Iliev, M. N.; Vergilov, I. V. *J. Phys. C: Solid State Phys.* **1988**, *21*, L199−L201.
(15) Yang, J.; Liu, H.; Martens, W. N.; Frost, R. L. *J. Phys. Chem. C* **2010**, *114*, 111−119.
(16) McIntyre, N. S.; Cook, M. G. *Anal. Chem.* **1975**, *47*, 2208−2213.
(17) Ismail, J. J.; Ahmed, M. F.; Kamath, P. V. *J. Solid State Chem.* **1995**, *114*, 550−555.
(18) Xu, B.; Bhawe, Y.; Davis, M. E. *Proc. Natl. Acad. Sci. U. S. A.* **2012**, *473*, 68−73.
(19) Tang, C.-W.; Wang, C.-B.; Chien, S.-H. *Thermochim. Acta* **2008**, *473*, 68−73.
(20) Yamada, Y.; Yano, K.; Hong, D.; Fukuzumi, S. *Phys. Chem. Chem. Phys.* **2012**, *14*, 5753−5760.
(21) Petitto, S.; Marsh, E. M.; Carson, G. A.; Langell, M. *J. Mol. Catal.* **2008**, *281*, 49−58.
(22) Hong, D.; Yamada, Y.; Nagatomi, T.; Takai, Y.; Fukuzumi, S. *J. Am. Chem. Soc.* **2012**, *134*, 19572−19575.
(23) Yang, C. C.; Eggenhuisan, T. M.; Wolters, M.; Agiral, M.; Frei, H.; de Jongh, P. E.; de Jongh, K. P.; Mul, G. *ChemCatChem* **203**, *5*, 550−556.
(24) Grzelczak, M.; Zhang, J.; Pfrommer, J.; Hartmann, J.; Driess, M.; Antonietti, M.; Wang, X. *ACS Catal.* **2013**, *3*, 383−388.
(25) Elizarova, G. L.; Matvienko, L. G.; Lozhkina, N. V.; Parmon, V. N. *React. Kinet. Catal. Lett.* **1988**, *36*, 331−336.
(26) Elizarova, G. L.; Matvienko, L. G.; Parmon, V. N. *J. Mol. Catal.* **1987**, *43*, 171−181.
(27) O'Day, P. A.; Brown, G. E.; Parks, G. A. *J. Colloid Interface Sci.* **1994**, *165*, 269−289.
(28) Ha, D.-H.; Moreau, L. M.; Honrao, S.; Hennig, R. G.; Robinson, R. D. *J. Phys. Chem. C* **2013**, *117*, 14303−14312.
(29) Xie, X.; Li, Y.; Liu, Z.-Q.; Haruta, M.; Shen, W. *Nature* **2009**, *458*, 746−749.